FINAL REPORT

Project Title: Radiation-Induced Segregation and Phase Stability in Candidate Alloys for the Advanced Burner Reactor

NERI 07-015

Covering Period: September 1, 2007 through February 28, 2011

Date of Report: May 29, 2011

Recipient: University of Michigan
2355 Bonisteel Blvd
Ann Arbor, MI 48109-2104

Award Number: DE-FC07-07ID14828

Principal Investigator: Gary S. Was, 734 763-4675, gsw@umich.edu
Co-PI: Brian D. Wirth, bdwirth@utk.edu

Collaborators: Stuart Maloy, LANL, maloy@lanl.gov;
Jeremy Busby, ORNL, busbjt@onrl.gov

Project Objective: The objective of this project is to determine the effect of irradiation on the segregation and phase stability in candidate alloys that may be used as structural materials for transmutation in the advanced burner reactor. This project will focus on ferritic-martensitic (F-M) alloys T91 and HT-9, an experimental oxide dispersion-strengthened (ODS) alloy, and an advanced austenitic alloy, D9, to investigate the electronic–magnetic–elastic interactions between chromium and radiation-induced defects. This project seeks to provide an understanding of radiation-induced segregation (RIS) and phase stability that can be used to develop predictive irradiation performance models.

Project Summary

Major accomplishments of this project were the following:

1) Radiation induced depletion of Cr occurs in alloy D9, in agreement with that observed in austenitic alloys.
2) In F-M alloys, Cr enriches at PAG grain boundaries at low dose (<7 dpa) and at intermediate temperature (400°C) and the magnitude of the enrichment decreases with temperature.
3) Cr enrichment decreases with dose, remaining enriched in alloy T91 up to 10 dpa, but changing to depletion above 3 dpa in HT9 and HCM12A.
4) Cr has a higher diffusivity than Fe by a vacancy mechanism and the corresponding atomic flux of Cr is larger than Fe in the opposite direction to the vacancy flux.
5) Cr concentration at grain boundaries decreases as a result of vacancy transport during electron or proton irradiation, consistent with Inverse Kirkendall models.
6) Inclusion of other point defect sinks into the KLMC simulation of vacancy-mediated diffusion only influences the results in the low temperature, recombination dominated regime, but does not change the conclusion that Cr depletes as a result of vacancy transport to the sink.
7) Cr segregation behavior is independent of Frenkel pair versus cascade production, as simulated for electron versus proton irradiation conditions, for the temperatures investigated.
8) The amount of Cr depletion at a simulated planar boundary with vacancy-mediated diffusion reaches an apparent saturation value by about 1 dpa, with the precise saturation concentration dependent on the ratio of Cr to Fe diffusivity.
9) Cr diffuses faster than Fe by an interstitial transport mechanism, and the corresponding atomic flux of Cr is much larger than Fe in the same direction as the interstitial flux.
10) Observed experimental and computational results show that the radiation induced segregation behavior of Cr is consistent with an Inverse Kirkendall mechanism.

1.0 Introduction

The objective of this project is to determine the effect of irradiation on the segregation and phase stability in candidate alloys that may be used as structural materials for transmutation in the advanced burner reactor. This project focused on ferritic-martensitic (F-M) alloys T91 and HT-9, an advanced F-M alloy, HCM12A, and an advanced austenitic alloy, D9. Originally, an ODS alloy was planned for study, but difficulty in obtaining material resulted in substitution of HCM12A for the ODS alloy. Also, since phase stability depends so strongly on RIS, the focus of this effort was to understand, explain and model RIS. The program consisted of an experimental phase and a modeling phase.

Quarterly reports submitted throughout the project provided detailed information on motivation, experimental procedures and a full description of all results obtained in the project. As such, this final report will focus on the major accomplishments of the project, and will not repeat procedures and presentation of all results. Rather, we will highlight the major accomplishments

and their significance. A list of all publications resulting from this project is also provided along with a final milestone chart.

2.0 Measurements of RIS in F-M alloys and in alloy D9

The objective of the experimental portion of this program was the determination of the radiation induced segregation in F-M alloys in a systematic way that also provided the dose and temperature dependence of the process. A second objective was the determination of the mechanism of RIS in these alloys. Sections 2.1 describe the outcome of the experimental results of the systematic study of RIS, and section 2.2 describes the mechanism of RIS.

2.1 Systematic measurements of Cr RIS in F-M alloys

The primary goal of this project was to measure and determine the process by which Cr segregates to grain boundaries in F-M alloys under irradiation. The first part of that objective is the systematic measurement of grain boundary Cr segregation.

Prior to this project, little was known or understood about radiation-induced segregation in F-M alloys. At the time, only a small body of literature reported experimental measurements of Cr RIS in F-M alloys; as summarized by Lu, *et al*. [1]. Of those studies, about half showed that chromium enriched under irradiation, while the other half exhibited chromium depletion However, no two experiments were performed under the same irradiation conditions— the alloy, dose, dose rate, temperature, irradiating particle were all different. Furthermore, not all of the studies reported on the grain boundary composition profile in the as-received condition. Recent work by Marquis and collaborators [2, 3] add further to the body of literature. In one study, Marquis, *et al*. [2] irradiated a Fe-14.25wt%Cr model alloy with 0.5 MeV and 2.0 MeV Fe^{+} ions. A pre-existing Cr concentration peak at grain boundaries was observed in the as-received alloy; following irradiation, 'W'-shaped profiles were observed, with the grain boundary Cr concentration being less than or equal to that in the unirradiated condition. The second study by Marquis, *et al*. [3] showed that a model ODS Fe-12Cr steel exhibited Cr enrichment in the as-received condition, then exhibited Cr depletion following irradiation with 0.5 MeV and 2.0 MeV Fe^{+} ions. Since the body of literature on Cr RIS in F-M alloys is small and unresolved, this project presented a more systematic approach to measure RIS of Cr in high purity Fe-Cr.

Three commercial F-M alloys (T91, HT9 and HCM12A), and one commercial austenitic alloy (D9), were studied in this project. Alloy HCM12A, was added to the project because of its potential use in fast reactor applications. The composition of all four alloys is given in Table 2.1. All alloys were irradiated with 2.0 MeV protons at a dose rate of approximately 10^{-5} dpa/sec at the Michigan Ion Beam Laboratory. Two experimental series, listed below, were designed to provide Cr RIS data for each alloy, both as a function of dose and of temperature.

- 400°C irradiation to 3, 7, and 10 dpa
- 500°C irradiation to 3, 7, and 10 dpa

Following initial analysis of the data, it was determined that an irradiation dose below 3 dpa was of interest in alloy T91, so another 2.0 MeV proton irradiation was carried out at 400°C to 1 dpa.

As expected with the austenitic alloy, D9, exhibited Cr RIS behavior very similar to that of typical austenitic stainless steels. Cr depletion was consistently observed on grain boundaries, and the amount of segregation increased with dose.

The F-M alloys exhibited a much more complex RIS behavior, exhibiting enrichment in some cases, and depletion in other cases. Alloy T91 consistently exhibited Cr enrichment at prior austenite grain boundaries (PAGBs), at both 400°C and 500°C, at all doses studied. The T91 Cr enrichment magnitude was small, never exceeding ~1.5 at%. The alloys HT9 and HCM12A exhibited Cr enrichment at 3 dpa, which reverted to Cr depletion at 7 dpa and 10 dpa. Both enrichment and depletion magnitudes were small in HT9 and HCM12A, never exceeding ~1.5 at%.

High dose ion irradiations were conducted using 5 MeV Fe^{++} at a dose rate of 10^{-3} dpa/s at temperatures that were designed to match either the RIS behavior (600°C) or the microstructure (440°C) of that from the lower dose rate proton irradiations. The irradiation conditions were:

- 440°C, 30 dpa
- 600°C, 14 dpa

Only alloy T91 was studied following these ion irradiations. The 440°C, 30 dpa irradiation produced approximately the same magnitude of Cr enrichment as the 400°C, 7 dpa proton irradiation. The 600°C, 14 dpa irradiation yielded no discernible segregation of Cr.

All experimental results are listed in Table 2.2, including the average Cr RIS magnitudes which were determined by experiment, the standard deviations of these magnitudes, the total number of grain boundaries studied, and the total number of line scans collected for the given condition. Representative RIS profiles for most of the conditions are shown in Figure 2.1.

The results provide a much-needed systematic study of RIS behavior in F-M alloys. Prior to this study, the body of existing experimental RIS data was disconnected; no conclusions could be drawn from it, and no behaviors could be identified. However, the results of this project have shown definite behaviors in RIS data, dependent upon dose, temperature, and bulk Cr concentration. The behaviors identified from the results of this project form a sound basis upon which future predictive RIS models can be built and compared.

2.1.1 Dose dependence of Cr RIS in F-M alloys

The second accomplishment of this project is the determination of dose and temperature dependence of Cr RIS. Austenitic steels typically exhibit Cr depletion, the magnitude of which tends to increase with increasing dose, until reaching a plateau. The plateau is achieved at the RIS steady-state dose, which typically occurs between 7 dpa and 10 dpa.

This study has confirmed that the austenitic alloy, austenitic D9, exhibits RIS behavior that is typical of austenitic steels. Figure 2.2 shows the average change in grain boundary Cr

concentration (wt%) for D9 irradiated at 400°C with 2.0 MeV protons. A small Cr depletion magnitude (~0.75 wt%) is observed at 3 dpa. But by 7 dpa, a much larger magnitude of Cr depletion is observed (~2.5 wt%); the change in Cr RIS magnitude between 3 dpa and 7 dpa is statistically resolvable, because the error bars of the two data points do not overlap. Between 7 dpa and 10 dpa, slightly more Cr depletion occurs, but the difference is not resolvable since the error bars of the two data points overlap significantly. This indicates that steady-state RIS has been achieved.

Conversely, the F-M alloys behave very differently from D9 and other austenitic alloys. A steady-state behavior is never observed in the F-M alloys. In addition, not all F-M alloys exhibit the same RIS behavior. The dose-dependent behavior of T91 is very different than the dose-dependent behavior of HT9 and HCM12A.

T91 exhibits Cr enrichment at all doses and temperatures studied. Figure 2.3a shows the average change in grain boundary Cr concentration (wt%) for T91 irradiated at 400°C and 500°C with 2.0 MeV protons. Cr RIS at both temperatures follows the same dose dependence, which can be described as follows. Small magnitudes of Cr enrichment (<1.5 wt%) are observed at doses ≤3 dpa. Between 3 dpa and 7 dpa, Cr RIS appears nearly unchanged; the average RIS magnitude is only slightly higher at 7 dpa than at 3 dpa, and the large error bars render that difference statistically insignificant. However, between 7 dpa and 10 dpa, a significant decrease in Cr enrichment magnitude is observed. These behaviors, as a function of dose, are the same at 400°C and 500°C.

HT9 and HCM12A have an even more complex RIS behavior, exhibiting both Cr enrichment and Cr depletion, Figure 2.3b. Following 2.0 MeV proton irradiation at 400°C to 3 dpa, both HT9 and HCM12A exhibit very small magnitudes of Cr enrichment (≤~0.5 wt%). Between 3 dpa and 7 dpa, both alloys switch from Cr enrichment to Cr depletion, exhibiting ~1 wt% Cr depletion at 7 dpa. Between 7 dpa and 10 dpa, HT9 may reach a steady-state behavior, because the average RIS magnitudes at these doses are very similar and have significant overlap of their error bars. This dose dependence at 400°C of HT9 and HCM12A is shown in Figure 2.4.

The complex Cr RIS behavior of the F-M alloys is likely due to their complex microstructural evolution. The F-M microstructure is far more complex than the austenitic microstructure, as it contains multiple types of boundaries (prior austenite, packet, lath, and subgrain), high-density networks of dislocations, dislocation loops, carbides on boundaries and in the matrix, and few-nanometer-sized precipitates rich in Ni, Si, Mn, and Cu. The evolution of each of these features is likely the cause of the change from enrichment to depletion in HT9 and HCM12A, and also likely the cause of the decrease in enrichment magnitude in T91.

2.1.2 Temperature dependence of Cr RIS in F-M Alloys

In austenitic alloys, RIS is maximized at an intermediate temperature. At very low temperatures, RIS is suppressed because of the immobility of the point defects. Conversely, at high temperatures, RIS is minimal because supersaturation of point defects is reduced and mobility is high so concentration gradients are difficult to support. Experiments in the temperature range

400-500°C have revealed that indeed, RIS is greater in the intermediate temperature range (~400°C) than at higher temperature (500°C).

For T91 at both 3 dpa and 7 dpa, Cr enrichment at 400°C significantly greater than the 500°C, Fig. 2.4. However, at 10 dpa, RIS at 500°C is greater than that at 400°C. But since 10 dpa is beyond the peak in segregation, this data is likely influenced by the irradiated microstructure, which may be different at the two temperatures.

A similar trend of decreasing Cr RIS magnitude with temperature is observed with the Fe^{++} ion irradiations. Although the 600°C irradiation was carried out to a higher dose than the 440°C irradiation, the general temperature dependence is still valid. The 30 dpa, 440°C irradiation exhibited an average Cr enrichment of ~1.5 wt%, whereas the 14 dpa, 600°C irradiation exhibited only ~0.3 wt% Cr enrichment. The error bars between the two temperature data points do not overlap, representing a statistically significant decrease in the RIS magnitude between 440°C and 600°C.

2.2 Interpreting RIS in F-M alloys as an Inverse Kirkendall process

Solute segregation in concentrated alloys has been attributed to differences in atom-defect exchange rates of constituent atoms via the inverse Kirkendall (IK) effect. Perks *et al*. [4] constructed a predictive model for RIS in austenitic Fe-Cr-Ni alloys based on the IK effect. This study utilized the Perks model [4] to determine RIS from solute exchange with point defect fluxes for F-M alloys.

The Perks model was adapted in this study for a binary Fe-9Cr BCC alloy, and implemented values of the input parameters that are appropriate for describing diffusion in Fe-9Cr alloys. The original equations of the Perks model remained unchanged for this study; they were solved for three constituent elements, but the binary composition was input by simply setting the concentration of the third constituent element to zero.

2.2.1 Temperature dependence

A series of IK model simulations investigated the temperature dependence of RIS, and were then compared to results from proton and Fe^{++} ion irradiation experiments on alloy T91. The temperature was varied between 300 and 600°C, with all other input parameters unchanged.

IK model results at $1x10^{-5}$ dpa/sec (comparable to the experimental proton dose rate) show that Cr enrichment occurs at grain boundaries at temperatures <530°C, and that Cr depletion occurs at temperatures >530°C. As shown in Figure 2.5a, this model-predicted temperature dependence is in agreement with experimental measurements from 7 dpa proton-irradiated T91, which exhibited a decrease in Cr enrichment magnitude with an increase in temperature between 400°C and 500°C. While sinks were initially neglected from the calculation (setting $\varrho_d = 0.0$ m^{-2}), inclusion of sinks in the IK model at an expected upper limit of $\varrho_d = 10^{17}$ m^{-2} brought the model result closer to the experimental data. The addition of sinks suppressed RIS, but Cr still enriched at lower temperatures and depleted at higher temperatures.

A similar temperature dependence is observed in the IK model of Fe-9Cr irradiated at a higher dose rate of 10^{-3} dpa/sec, which corresponds to the experimental Fe^{++} ion dose rate, Figure 2.5b. Cr enriches at low temperatures, the segregation magnitude decreases with increasing temperature, and Cr depletes at higher temperatures. The inclusion of sinks at $\varrho_d = 1x10^{17}$ m^{-2} moves the slope of the model-predicted Cr RIS vs. temperature curve into better agreement with the slope of the experimental data.

The change from Cr enrichment to Cr depletion in the IK model is attributed to the intersection of Cr:Fe diffusivity ratios of vacancies and interstitials. At temperatures where Cr enrichment occurs, the Cr:Fe diffusivity ratio of interstitials is greater than the Cr:Fe diffusivity ratio of vacancies; for every Cr atom that leaves the grain boundary via vacancy exchange, more than one Cr atom arrives at the boundary via interstitial migration, thus giving rise to a net Cr enrichment at the boundary. Likewise, at temperature where Cr depletion occurs, the Cr:Fe diffusivity ratio of interstitials is less than that of vacancies. This shows that both interstitials and vacancies play an important role in RIS of F-M alloys, unlike in austenitic steels, where the vacancies alone can sufficiently describe RIS behaviors.

2.2.2 Composition dependence

A series of IK model simulations investigated composition dependence of RIS for Fe-Cr alloys having a range of bulk Cr concentrations, from 9 to 15 at%, and were then compared to proton-irradiated experiments on alloys T91, HCM12A, and HT9. Chromium composition-dependent interstitial migration energies were utilized in the IK model. As shown in Figure 2.6, the IK model predicts decreasing Cr enrichment with increasing Cr concentration, similar to the experimental results. However, the slope of the modeled Cr RIS vs. bulk composition curve better fits the experimental data when sinks are included at the upper limit of their equivalent line density, or $\varrho_d = 1x10^{17}$ m^{-2}.

The necessity of composition-dependent interstitial migration energies further supports the argument that interstitials play a critical role in RIS in F-M alloys. Unlike in austenitic IK modeling, the interstitials cannot be ignored.

2.2.3 Dose dependence

The IK model predicted monotonically increasing Cr enrichment, with dose, up to a saturation or steady-state dose. Figure 2.7 illustrates this behavior in the proton reference case. The model-predicted direction of segregation (enrichment) agreed with experimental results; but neither the model-predicted RIS magnitude, nor the model-predicted dose dependence of RIS, agreed with experimental observations. The inclusion of sinks at a density $\varrho_d = 10^{17}$ m^{-2} caused less enrichment to occur, thus pushing model-predicted RIS magnitudes into better agreement with experimental results. But even with sinks, the model did not exhibit the experimentally observed trend of low-dose Cr enrichment, followed by either less enrichment or even depletion at higher doses.

It is likely that the dose dependence of F-M alloys cannot yet be captured by the IK model alone. Work in this project has shown a complex irradiation-induced microstructural evolution of F-M alloys, including the following: dislocation loop nucleation and growth, carbide growth and coarsening at PAGB and lath boundaries, matrix carbide growth and coarsening, Cu-rich precipitate nucleation and growth, and Ni-Si-Mn precipitate nucleation and growth. The interrelationship of these microstructural changes with RIS is not yet understood, and may play a significant role in the dose dependence of RIS. The IK model is not yet able to account for all of these changes, and therefore predicts the monotonic increase of segregation with dose.

References

[1] Z. Lu, R.G. Faulkner, G. Was and B.D. Wirth. *Irradiation-induced grain boundary chromium microchemistry in high alloy ferritic steels*. Scripta Materialia. 58 (2008) 878.

[2] E.A. Marquis, R. Hu and T. Rousseau. *A systematic approach for the study of radiation-induced segregation/depletion at grain boundaries in steels*. J. Nucl. Mater. 413 (2011) 1.

[3] E.A. Marquis, S. Lozano-Perez and V. de Castro. *Effects of heavy-ion irradiation on the grain boundary chemistry of an oxide-dispersion strengthened Fe-12wt.%Cr alloy*. J. Nucl. Mater. In press, accepted manuscript. doi: 10.1016/j.jnucmat.2010.12.251.

[4] Perks, J.M., Marwick, A.D. and English, C.A., *AERE R*, 1986, June, 12121.

Table 2.1. Composition (at%) of alloys studied in project

Element	Fe	Cr	Mo	Mn	Ni	V	Cu	W	Si	Nb	C	Ti
T91	89.15	8.37	0.9	0.45	0.21	0.216	0.17	--	0.28	0.076	0.1	--
HCM12A	84.22	10.83	0.3	0.64	0.39	0.19	1.02	1.89	0.27	0.054	0.11	--
HT9	84.92	11.63	1	0.52	0.5	0.3	0.04	0.52	0.22	--	0.2	<0.01
D9	65.64	13.95	2.20	2.03	15.12	<0.02	0.005	--	0.66	<0.02	0.043	0.26

Table 2.2. Summary of all irradiation conditions studied. Average Cr RIS magnitudes are listed with ± their standard deviation. Numbers in square brackets are the number of grain boundaries studied and the total number of line scans collected on those boundaries.

Alloy	Temp. (°C)	1 dpa	3 dpa	7 dpa	10 dpa	14 dpa	30 dpa
T91	400	0.56 ± 0.44 [2, 6	1.29 ± 0.37 [3, 14]	1.37 ± 0.44 [2, 9]	0.80 ± 0.20 [3, 11]	N/A	N/A
T91	500	N/A	0.99 ± 0.17 [2, 9]	1.08 ± 0.15 [2, 8]	0.87 ± 0.23 [2, 7]	N/A	N/A
T91	440 (Fe^{++})	N/A	N/A	N/A	N/A	N/A	1.40 ± 0.55 [2, 15]
T91	600 (Fe^{++})	N/A	N/A	N/A	N/A	0.33 ± 0.15 [2, 15]	N/A
HCM12A	400	TBD	0.33 ± 0.15 [2, 7]	-0.79 ± 0.18 [2, 9]	TBD	N/A	N/A
HCM12A	500	N/A	TBD	-2.02 ± 0.71 [2, 5]	TBD	N/A	N/A
HT9	400	TBD	0.56 ± 0.16 [4, 15]	-0.92 ± 0.16 [2, 7]	-0.96 ± 0.13 [5, 16]	N/A	N/A
HT9	500	N/A	TBD	TBD	TBD	N/A	N/A
D9	400	TBD	-0.75 ± 0.19 [3, 10]	-2.45 ± 0.40 [2, 9]	-2.95 ± 0.57 [2, 8]	N/A	N/A
D9	500	N/A	TBD	TBD	TBD	N/A	N/A

TBD = irradiated, but RIS measurement not collected
N/A = not irradiated at this condition

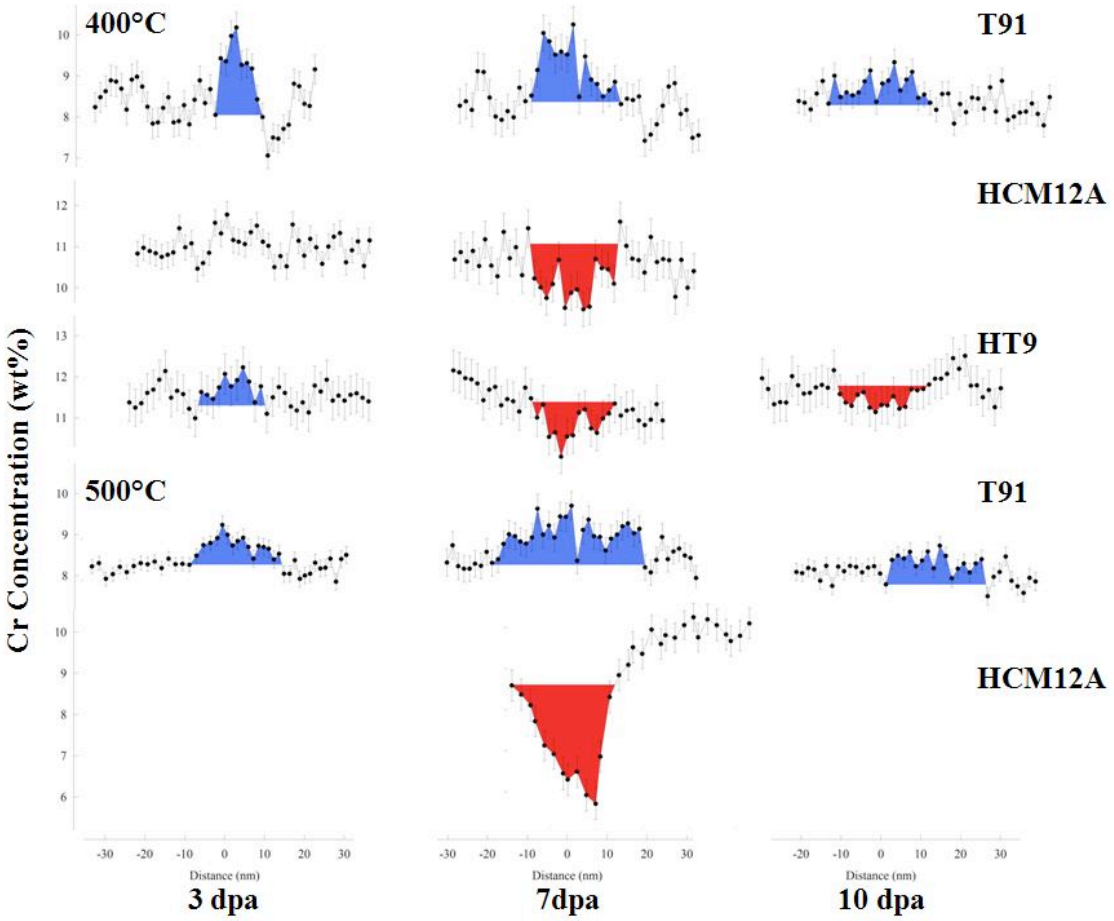

Figure 2.1. Representative RIS profiles for F-M irradiation conditions studied.

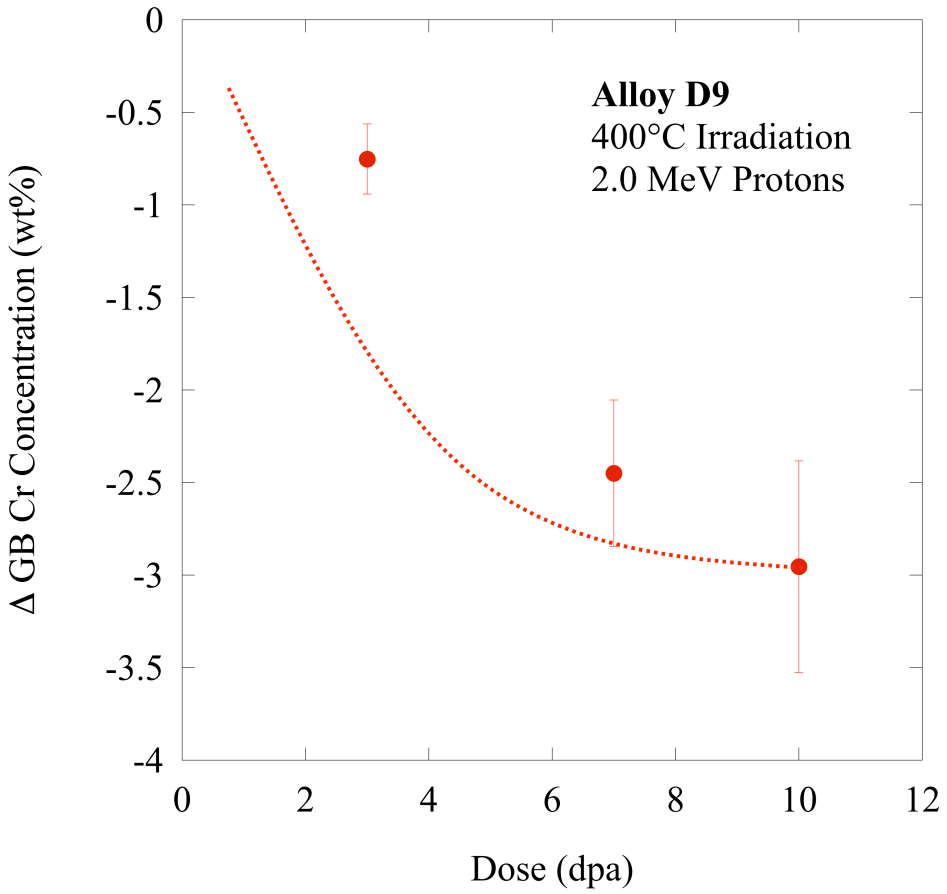

Figure 2.2. Average change in grain boundary Cr concentration (wt%) of alloy D9, irradiated at 400°C with 2.0 MeV protons. D9 exhibits Cr depletion, and reaches RIS steady-state between 7 and 10 dpa.

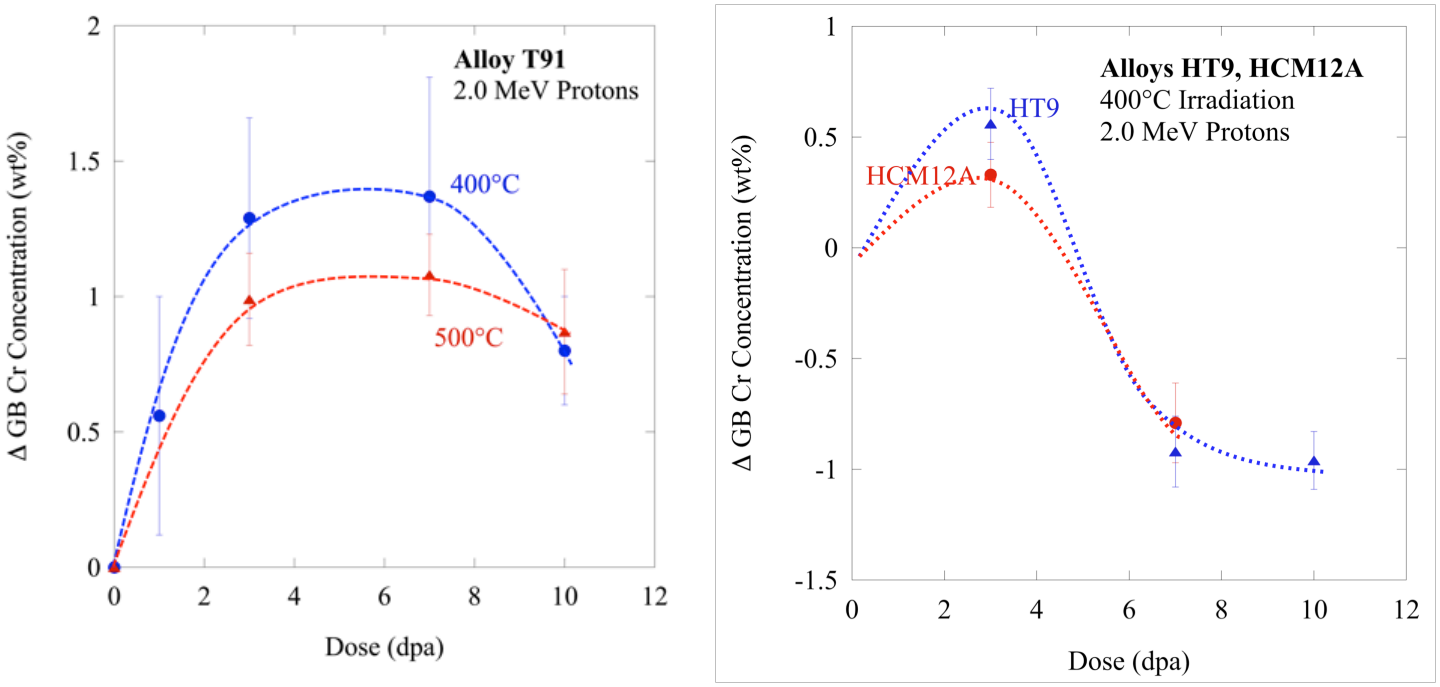

Figure 2.3. Average change in grain boundary Cr concentration (wt%) of (a) alloy T91, and (b) alloys HT9 and HCM12A irradiated with 2.0 MeV protons.

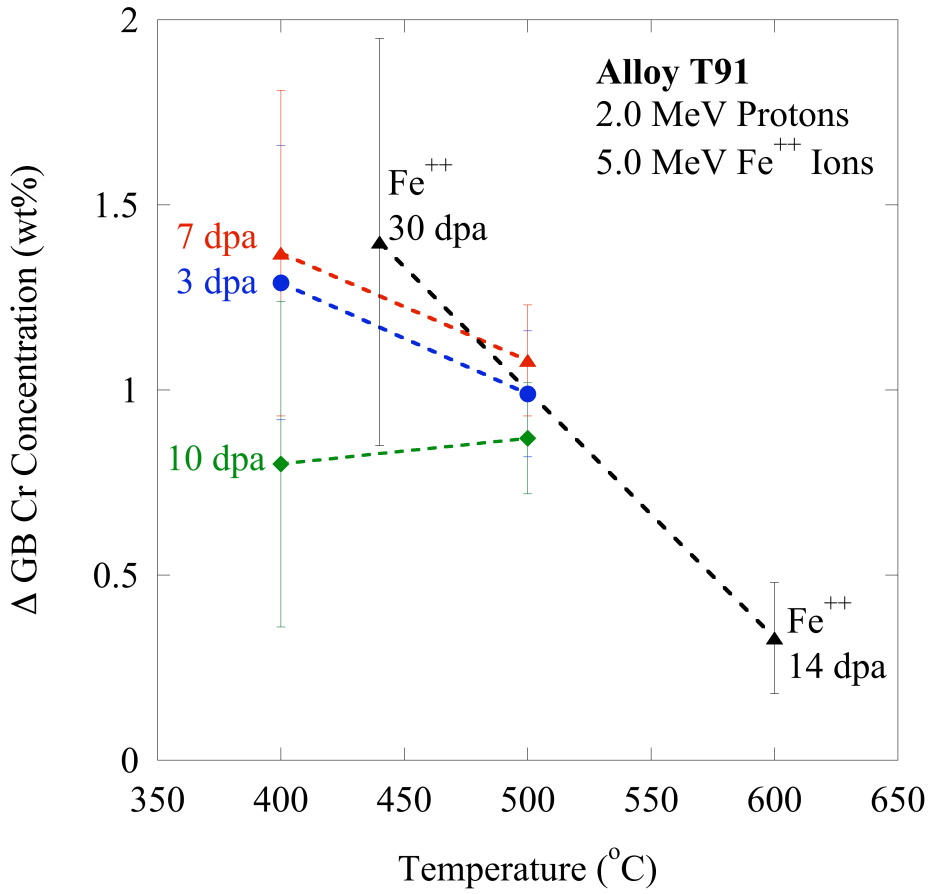

Figure 2.4. Average change in grain boundary Cr concentration (wt%) of alloy T91, irradiated at 400°C and 500°C with 2.0 MeV protons to different doses, and at 440°C and 600°C with 5.0 MeV Fe^{++} ions. General behavior is that Cr RIS magnitude decreases with increasing temperature.

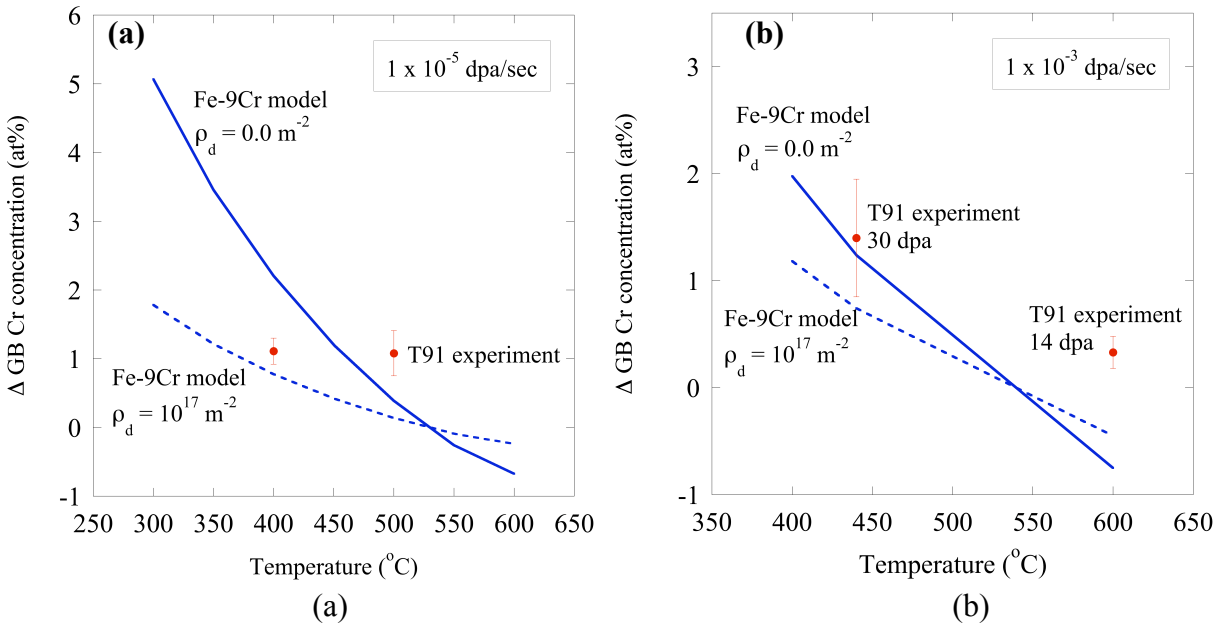

Figure 2.5. Inverse Kirkendall model result for Fe-9Cr at (a) 10^{-5} dpa/sec and (b) 10^{-3} dpa/sec compared to the experiments under the same conditions.

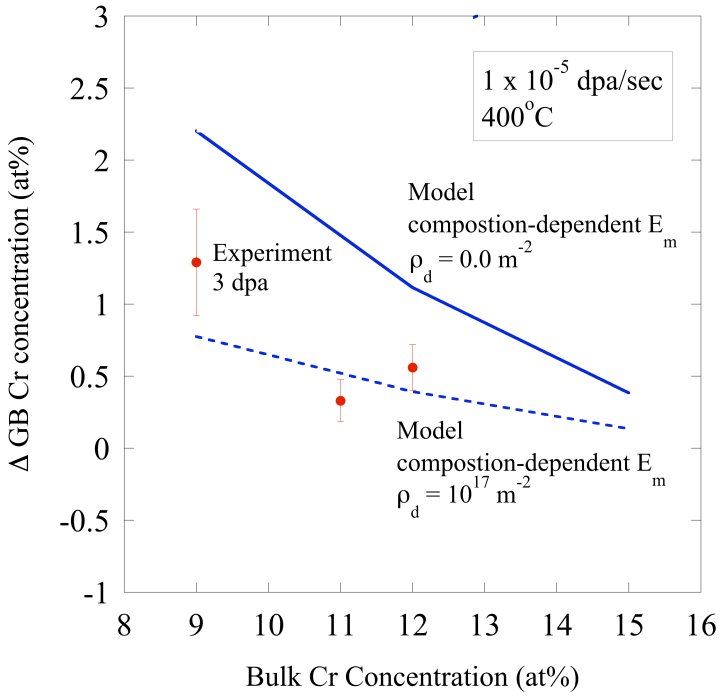

Figure 2.6. Inverse Kirkendall model for 400°C irradiation at 10^{-5} dpa/sec predicts same bulk Cr concentration dependence as observed in 3 dpa proton irradiation experiments on T91, HCM12A, and HT9.

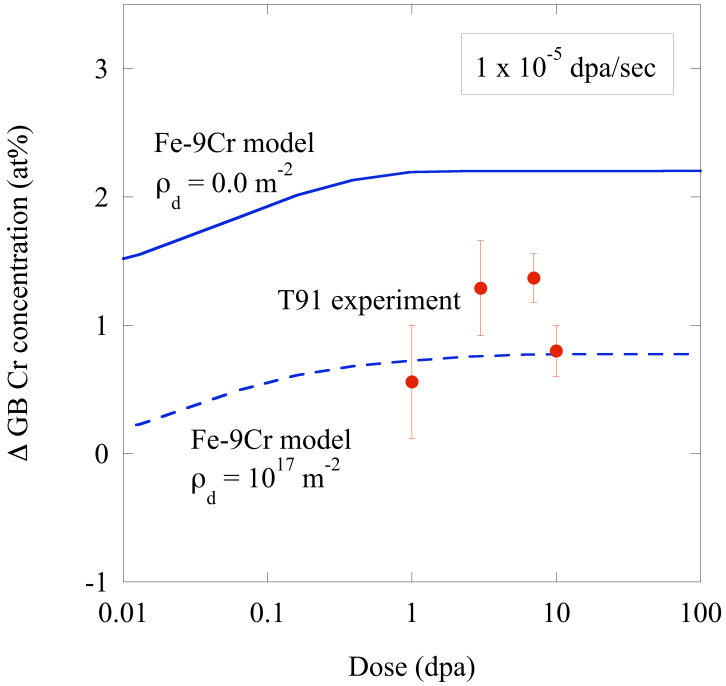

Figure 2.7. Inverse Kirkendall model for 400°C irradiation at 10^{-5} dpa/sec predicts monotonic increase to steady-state as a function of dose, which is unlike the dose dependence observed in proton-irradiated T91.

3.0 Modeling RIS in F-M Alloys

Kinetic lattice Monte Carlo (KLMC) models have been developed, within a multiscale materials modeling framework, to simulate the flux of radiation-induced defects to a perfectly absorbing planar sink in body-centered cubic (BCC) Fe-Cr alloys. These simulations naturally capture the detailed thermodynamics of point-defect solute interactions and the coupling of the solute to point defect fluxes required to predict the radiation-induced segregation behavior of Cr. This leads to the possibility that the mixed enrichment and depletion behavior of radiation-induced Cr segregation could be explained based on the differences in interstitial versus vacancy fluxes to a given boundary. However, additional modeling work is required to fully quantify the anticipated Cr segregation behavior as a function of grain boundary character and irradiation conditions. The remainder of this section will very briefly review the separate KLMC models for vacancy and interstitial diffusion, respectively, followed by a section describing the key results.

Two distinctly different kinetic lattice Monte Carlo (KLMC) models were developed within this project to simulate the coupling between point defect and solute fluxes to a planar sink and the corresponding radiation-induced segregation of Cr in BCC Fe-Cr alloys by vacancy- or interstitial-mediated transport mechanism. Either electron or proton irradiation can be simulated in this model. Electron irradiation is simulated by the insertion of a single Frenkel pair, consisting of a vacancy and interstitial dumbbell pair, into the lattice system. The proton irradiation simulations involve a bit more complicated defect introduction. The SRIM binary collision code [1] has been used to determine the partitioning of the kinetic energy of the proton between electronic and nuclear stopping, as well as to determine the energy distribution of primary knock-on atoms (PKAs). Figure 3.1 shows the cumulative probability distribution of PKA energy created by 2 MeV protons at a depth of 10 microns below the surface where the dpa production rate is uniform. The PKA energy is then sampled in the KLMC simulation to determine the spatial distributions of vacancies, or interstitials, to introduce at the appropriate rate. The spatial distributions of defects created by an energetic displacement cascade have been obtained from a molecular dynamics database of cascade evolution in body-centered cubic iron performed by Stoller [2]. If a defect distribution does not exist for the particular PKA energy chosen by a random number from the cumulative distribution function obtained from SRIM, then a cascade from the database with the closest corresponding PKA energy is used instead.

Vacancy-mediated KLMC transport

The KLMC model simulates damage evolution in Fe-Cr alloys by following vacancy – nearest neighbor atom exchanges on a bcc lattice, beginning from the spatial vacancy population produced under irradiation at a dose rate of 1.3×10^{-5} dpa/sec to the ultimate annihilation of vacancies, either due to reaction at imposed sinks or at the simulation cell boundary. Two of the three boundaries are treated as periodic, while the third direction has a perfect black absorbing sink meant to simulate a high angle grain boundary. The KLMC boundary conditions remove (annihilate) a vacancy upon contact, and track the solute re-distribution as a function of dose as the vacancies diffuse through the lattice.

The potential energy of the local vacancy – Cr – Fe environment determines the relative vacancy jump probability to each of the eight possible nearest neighbors in the bcc lattice. The unrelaxed Fe – Cr - vacancy lattice energetics are described using Finnis-Sinclair N-body type potentials. The chromium and iron potentials are from Finnis and Sinclair [3] and Ackland et. al [4],

respectively; and two different iron-chromium potentials were fit to provide either slightly under- or over-sized Cr atom interactions, as described by Shim et al. [5].

Interstitial-mediated KLMC transport
A new KLMC model has been developed to simulate interstitial mediated transport. Single dumbbell interstitials are inserted into the lattice and assumed to have one of three <110>-orientations, namely [110], [101] or [011]. The dumbbells and the resulting lattice strain at neighboring atom positions are not explicitly incorporated, rather a given lattice site is assigned to be a dumbbell interstitial, with a given <110> orientation and by defining whether the dumbbell consists of two atoms sharing a single lattice site that are Fe-Fe, mixed Fe-Cr, or Cr-Cr. The dumbbell interstitial is allowed to move to any of the eight nearest neighbor positions.

When a dumbbell interstitial jumps from one lattice position to a neighboring position, only one of the two atoms that make up the dumbbell actually moves to that new position, while the other atom returns to the lattice site of the original interstitial position. The atom that jumps from one site to the next is geometrically determined by the orientation of the dumbbell and the specific nearest neighbor jump selected by the stochastic algorithm. In the case of interstitial dumbbell mediated transport, the change in energy used to determine which neighboring position is selected for a jump is obtained by a sum of the lattice potential energy determined by the spatial position of all atoms plus an additional potential energy associated with whether the interstitial consists of an Fe-Fe (4.8 eV), Fe-Cr (4.7 eV) or Cr-Cr (4.6 eV) dumbbell. These values provide an energetic bias for the formation of mixed or Cr-Cr dumbbells and the magnitude of these energy differences are consistent with the results of ab-initio [9] and molecular dynamics simulations [8]. To date, the interstitial mediated transport has only been applied for the case of electron irradiation and the formation of interstitial clusters, which migrate in a one-dimensional manner along the direction of the Burgers vector rather than three-dimensionally has not been considered.

3.1 Modeling Results and Discussion

3.1.1 Faster Cr diffusion and radiation-induced depletion of Cr

Figure 3.2 summarizes the observed grain boundary concentration of Cr predicted by the vacancy-mediated KLMC code for conditions of electron irradiation at a dose rate of 1.3×10^{-5} dpa/s and a range of temperatures. In these simulation results, the loss of vacancies as a result of recombination or annihilation at fixed sinks besides grain boundaries has not been included. The specific interatomic potential used in this model predicts that Cr is slightly oversized with a small binding energy to the vacancy, which results in Cr being a faster diffuser than Fe. In this series of KLMC simulations, two different values of the saddle point energy, E*, have been used to describe the Cr – vacancy exchanges. In the first case, the E* value has been set to a value of 0.9 eV for vacancy exchanges with both Fe and Cr, and these cases are shown by the yellow, purple and blue lines at 100, 500 and 1000°C, respectively. The specific ratio of Fe/Cr diffusion obtained in the simulation is also shown in the figure. This diffusivity ratio naturally varies as a function of temperature and demonstrates that the KLMC model is successfully able to capture a temperature dependent correlation factor for vacancy-Cr exchanges. The second set of simulations set the value of E* for Cr-vacancy exchanges to be 0.15 eV lower than that of Fe-vacancy exchanges to a value of 0.75 eV, consistent with previous ab-initio calculations [9].

In both cases, Cr diffuses faster than Fe, and consistent with an inverse Kirkendall model, the Cr is observed to deplete at the grain boundary. Notably, however, the segregation behavior predicted by the KLMC model is seen to saturate very quickly as a function of irradiation dose. The absolute magnitude of the segregation is determined by the ratio of Fe/Cr diffusivity, as expected.

3.1.2 Incorporation of other point defect sinks into the KLMC model

Figure 3.3 shows the effect of including other vacancy loss mechanisms into the simulation results at an irradiation temperature of 100 or 200°C in an Fe-10%Cr alloy subject to electron irradiation at a dose rate of $1.3x10^{-5}$ dpa/sec, at 100°C (left) and 200°C (right). As mentioned in previous reports, the additional sinks consist of vacancy-interstitial recombination and absorption at dislocations. These sinks are not explicitly included in the spatial model, rather the volumetric reaction rates calculated from a steady state kinetic rate theory analysis are used to define the probability that a defect is annihilated (removed from the simulation) in any given step.

The red curve in each plot of Figure 3.3 shows the KLMC simulation results with the grain boundary as the only vacancy sink (besides self-clustering), whereas the blue curve shows the predicted grain boundary Cr concentration when including recombination and vacancy absorption at dislocations, with a dislocation density of 10^8 cm^{-2}. As expected, recombination is a dominant loss mechanism at low temperatures and there is a substantial difference in the flux of vacancies to the grain boundary and corresponding Cr depletion as a function of dose at 100°C. However, by 200°C, the amount of recombination has dropped considerably and the results are very comparable with and without the additional vacancy loss mechanisms in the KLMC model.

3.1.3 Effect of proton versus electron irradiation

Figure 3.4 shows a comparison of Cr segregation predicted for proton versus electron irradiation at a dose rate of $1.3x10^{-5}$ dpa/sec and an irradiation temperature of 500 or 1000°C. The red and green curves describe electron irradiation at 1000 and 500°C, respectively, whereas the blue and brown curves describe the case of proton irradiation. Notably, at these temperatures and dose rates, there is essentially no difference in the vacancy flux to the grain boundaries, and corresponding Cr depletion behavior. The reason for this likely relates to the relatively weak binding of vacancy clusters, which are observed to form in the case of proton irradiation, but at very small sizes of 2 – 5 vacancies. At these temperatures, the resulting vacancy clusters are thermally unstable and rapidly dissolve. Therefore, the simulations of both proton and electron irradiation predict similar vacancy fluxes to the grain boundary and corresponding Cr depletion at the boundary. Again, the Cr depletion is observed to quickly saturate as a function of irradiation dose and is a strong function of the diffusivity ratio between Fe and Cr.

3.1.4 Faster Cr diffusion by interstitial transport

Figure 3.5 shows results obtained from the KLMC model for interstitial-mediated transport. In this case, the Cr grain boundary concentration is not plotted, but rather Figure 3.5 plots the net flux of interstitials and Cr atoms through the simulation volume. The KLMC simulation was performed at a temperature of 1000°C for conditions of electron irradiation at a dose rate of $1.3x10^{-5}$ dpa/sec and to a dose of 4 dpa. The results show a strong coupling of the interstitial and

Cr atom flux and an Fe to Cr diffusivity ratio of 0.055 was obtained. Therefore, in this simulation, the Cr diffuses much faster (~20x) than Fe, which is somewhat surprising since molecular dynamics simulations performed at similar conditions indicate that Cr diffuses about 30% faster than Fe [8]. Therefore, the results on interstitial mediated transport are still being evaluated and compared to simulations performed at other irradiation temperatures. However, the results do indicate that the atomic flux that moves to the grain boundaries is dominated by Cr, with about 65% of the atomic flux moving in the same direction as the interstitials was Cr versus about 35% for Fe. Such strong atomic flux differences would clearly drive Cr enrichment at the grain boundary, and when coupled with the vacancy mediated transport that leads to Cr depletion, offers the possibility of being able to explain the varied experimental results which show a combination of enrichment and depletion.

However, additional modeling work is required to fully quantify the anticipated Cr segregation behavior as a function of grain boundary character and irradiation conditions. In particular, the interstitial-mediated KLMC model requires further verification and validation before performing an extensive set of simulations to quantify the coupling of the Cr versus Fe atomic fluxes to the interstitial fluxes. Likewise, the vacancy-mediated KLMC model predictions should be evaluated in terms of the vacancy fluxes and coupled atomic flux ratios, which are in the opposite direction. It is then anticipated that spatially-dependent reaction-diffusion equations should be solved to derive the vacancy and interstitial fluxes to grain boundaries as a function of grain boundary character and sink characteristics and irradiation conditions. These flux levels could then be coupled through the KLMC model results to predict the corresponding atomic fluxes and grain boundary chemistry changes. Thus, additional effort is required to quantify the grain boundary sink characteristics and to perform the reaction-diffusion model calculations.

References

[1]. J.F. Ziegler et al., 2010, "SRIM – The stopping and range of ions in matter (2010)", *Nuclear Instruments and Methods in Physics Research B,* **268,**
[2]. Stoller, R.E., 2000, "The role of cascade energy and temperature in primary defect formation in iron", *J. Nuc. Mat.,* **276**, 22.
[3]. M. W. Finnis and J. E. Sinclair, Phil. Mag. A 50 (1) (1984) 45.
[4]. G. J. Ackland, G. I. Tichy, V. Vitek, and M. W. Finnis, Phil. Mag. A 56 (1987) 735.
[5]. J.-H. Shim, H.-J. Lee and B.D. Wirth, "Molecular dynamics simulation of primary irradiation defect formation in Fe-10%Cr", J. Nucl. Mater. 351 (2006) 56.
[6]. M. P. Allen and D. J. Tildesley, "Computer Simulation of Liquids", Clarendon Press, Oxford (1990).
[7]. P.R. Monasterio, B.D. Wirth and G.R. Odette, "Kinetic Monte Carlo modeling of cascade aging and damage accumulation in Fe-Cu alloys", J. Nucl. Mater. 361 (2007) 127.
[8]. K.L. Wong, H.-J. Lee, J.-H. Shim, B. Sadigh, and B.D. Wirth, "Multiscale modeling of point defect interactions in Fe-Cr alloys", J. Nucl. Mater. 386-388 (2009) 227-230.
[9]. "Ab initio study of Cr interactions with point defects in bcc Fe", P. Olsson et al., Physical Review B 75.

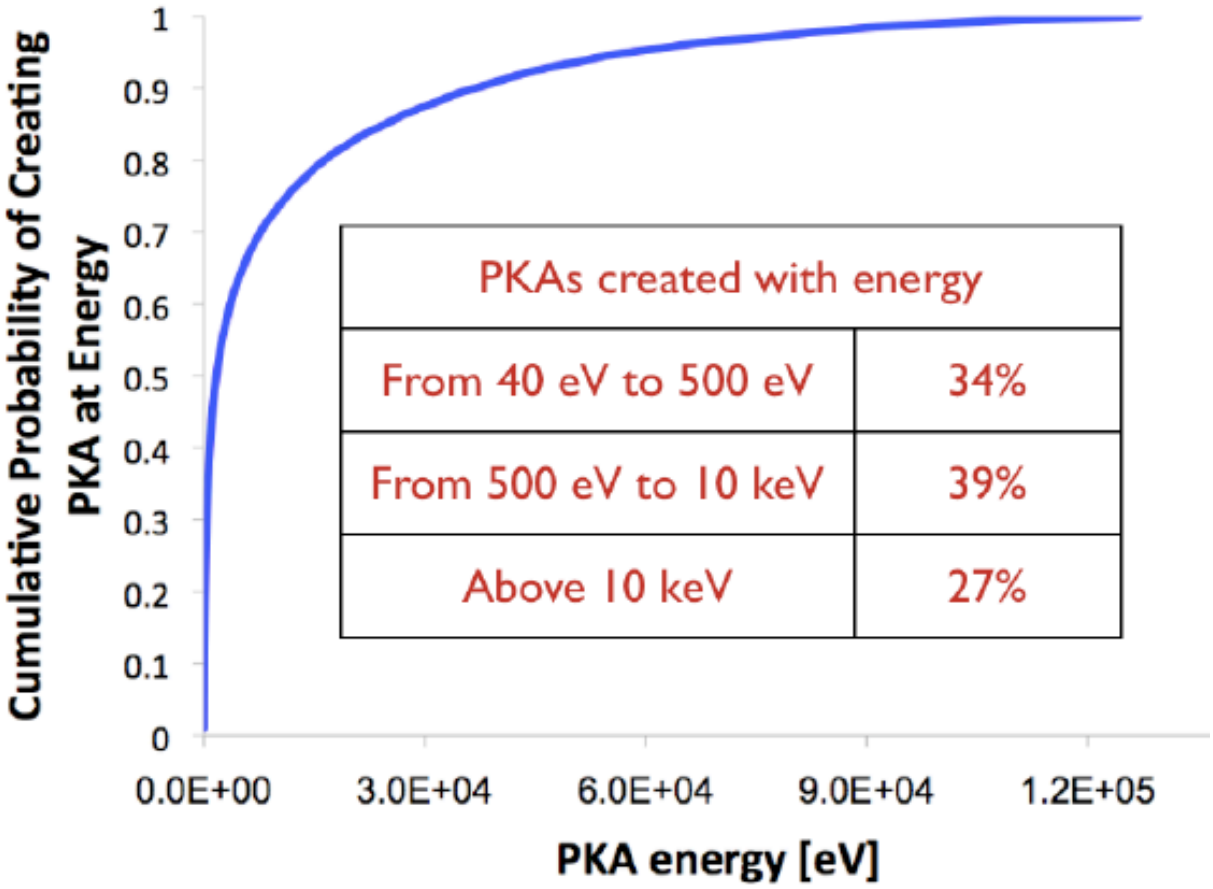

Figure 3.1. The PKA energy cumulative probability distribution for 2 MeV proton irradiation of an Fe-10%Cr alloy at a depth 10 microns below the surface, as calculated using SRIM [1].

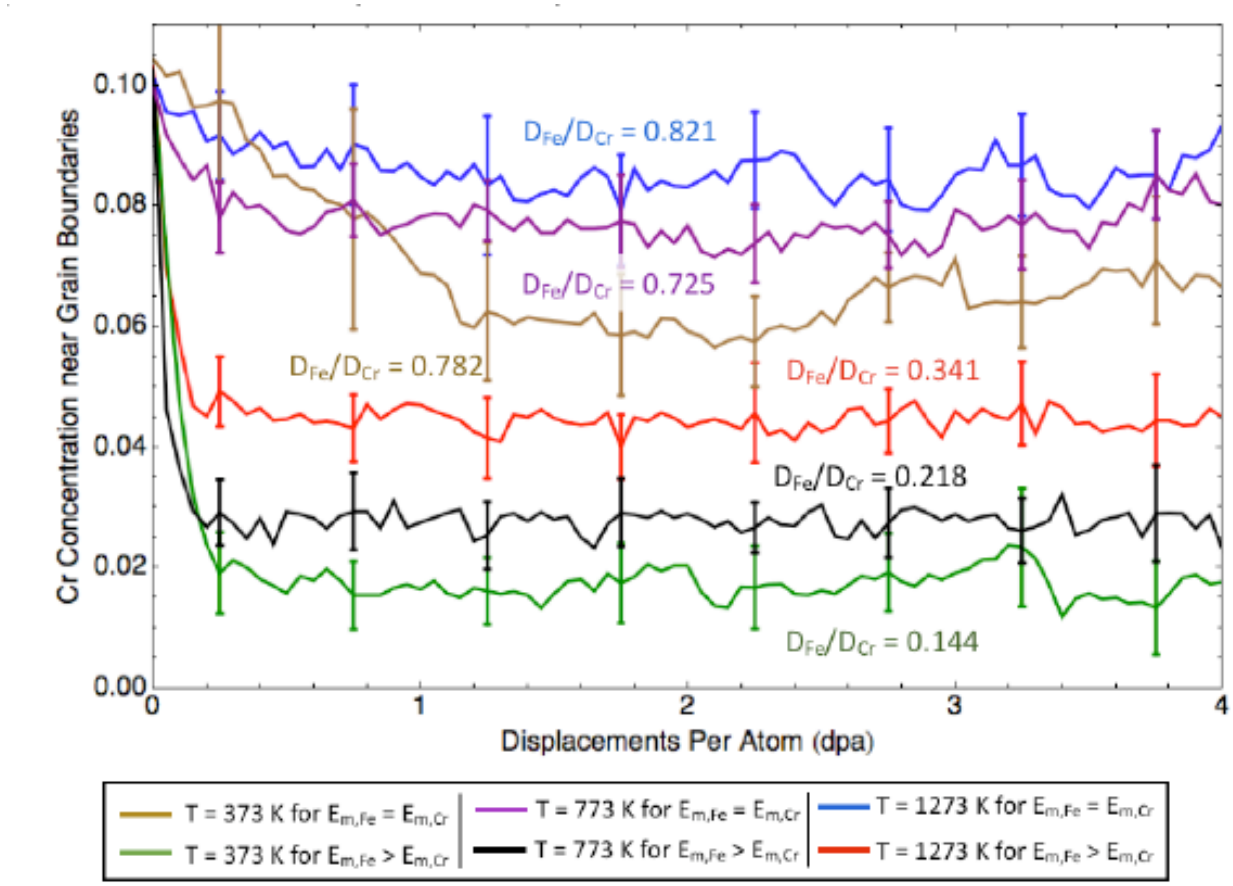

Figure 3.2. Vacancy-mediated KLMC model predictions for Cr concentration near the grain boundary in an Fe-10%Cr alloy subject to electron irradiation at a dose rate of 1.3×10^{-5} dpa/sec, and a range of temperatures from 100 to 1000°C. The specific model predicts that Cr is a faster diffuser than Fe, in agreement with ab-initio calculations, and demonstrate Cr depletion at the grain boundary consistent with an inverse Kirkendall model. Notably the segregation behavior rapidly saturates as a function of irradiation dose.

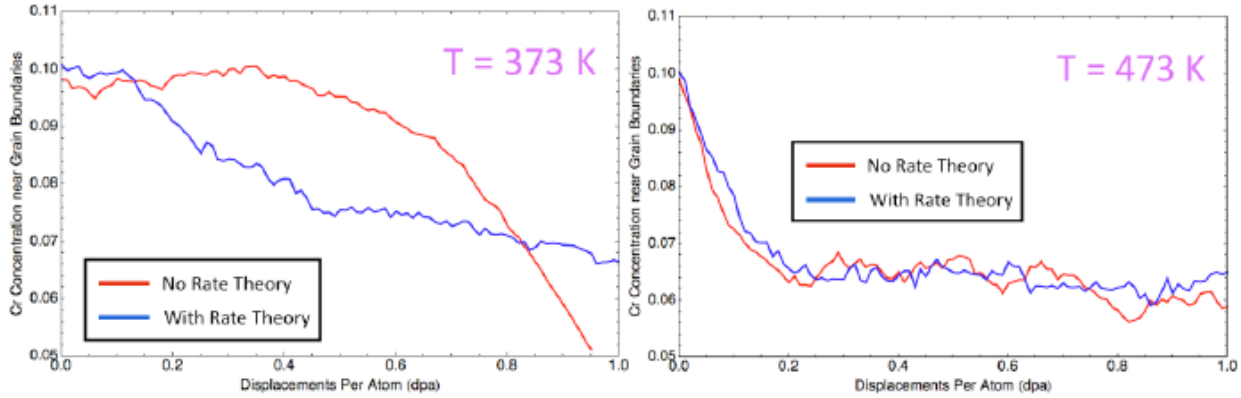

Figure 3.3. Vacancy-mediated KLMC model predictions of Cr concentration near the grain boundary in an Fe-10%Cr alloy subject to electron irradiation at a dose rate of 1.3×10^{-5} dpa/sec, at 100°C (left) and 200°C (right). The red curve in each plot shows the results of the simulations with the only vacancy sink being the grain boundary, whereas the blue curve shows the predicted grain boundary Cr concentration when including recombination and vacancy absorption at dislocations, with a dislocation density of 10^{8} cm^{-2}.

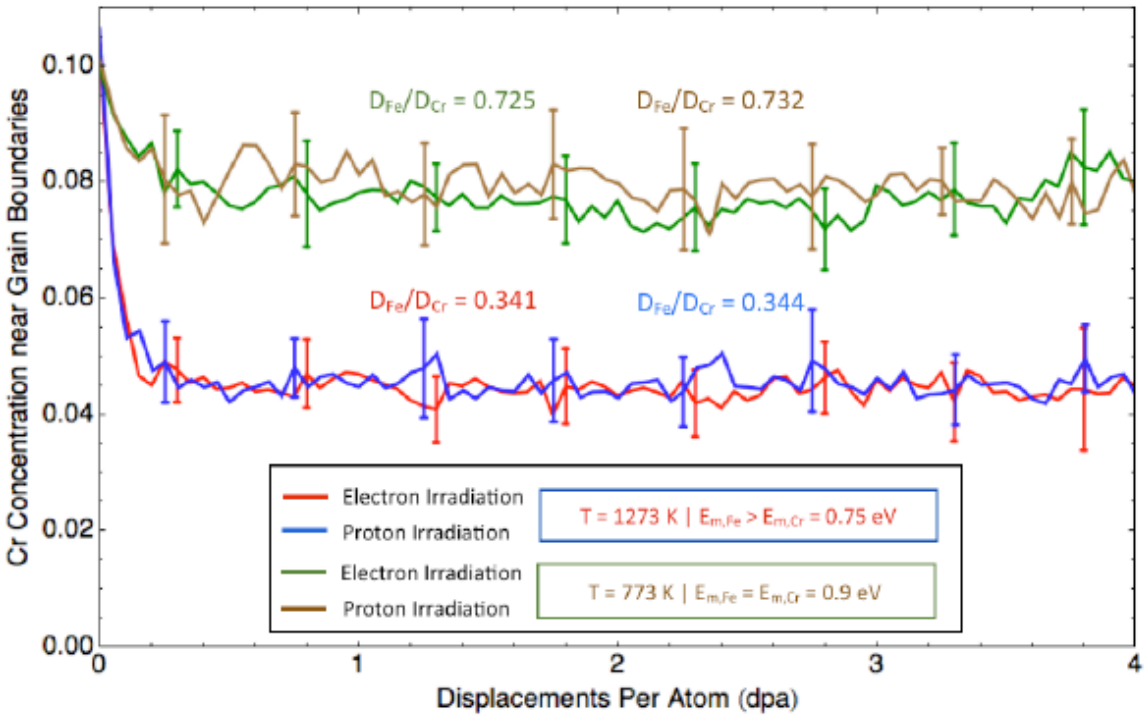

Figure 3.4. Vacancy-mediated KLMC model predictions of Cr concentration near the grain boundary as a function of dose in an Fe-10%Cr alloy subject to either electron or proton irradiation at a dose rate of 1.3×10^{-5} dpa/sec. The red and green curves describe electron irradiation at 1000 and 500°C, respectively, whereas the blue and brown curves describe the case of proton irradiation. Notably, at these temperatures and dose rates, there is essentially no difference in the vacancy flux to the grain boundaries, and corresponding Cr depletion behavior. The ratio of Fe/Cr diffusivity is shown on the figure for each simulation result.

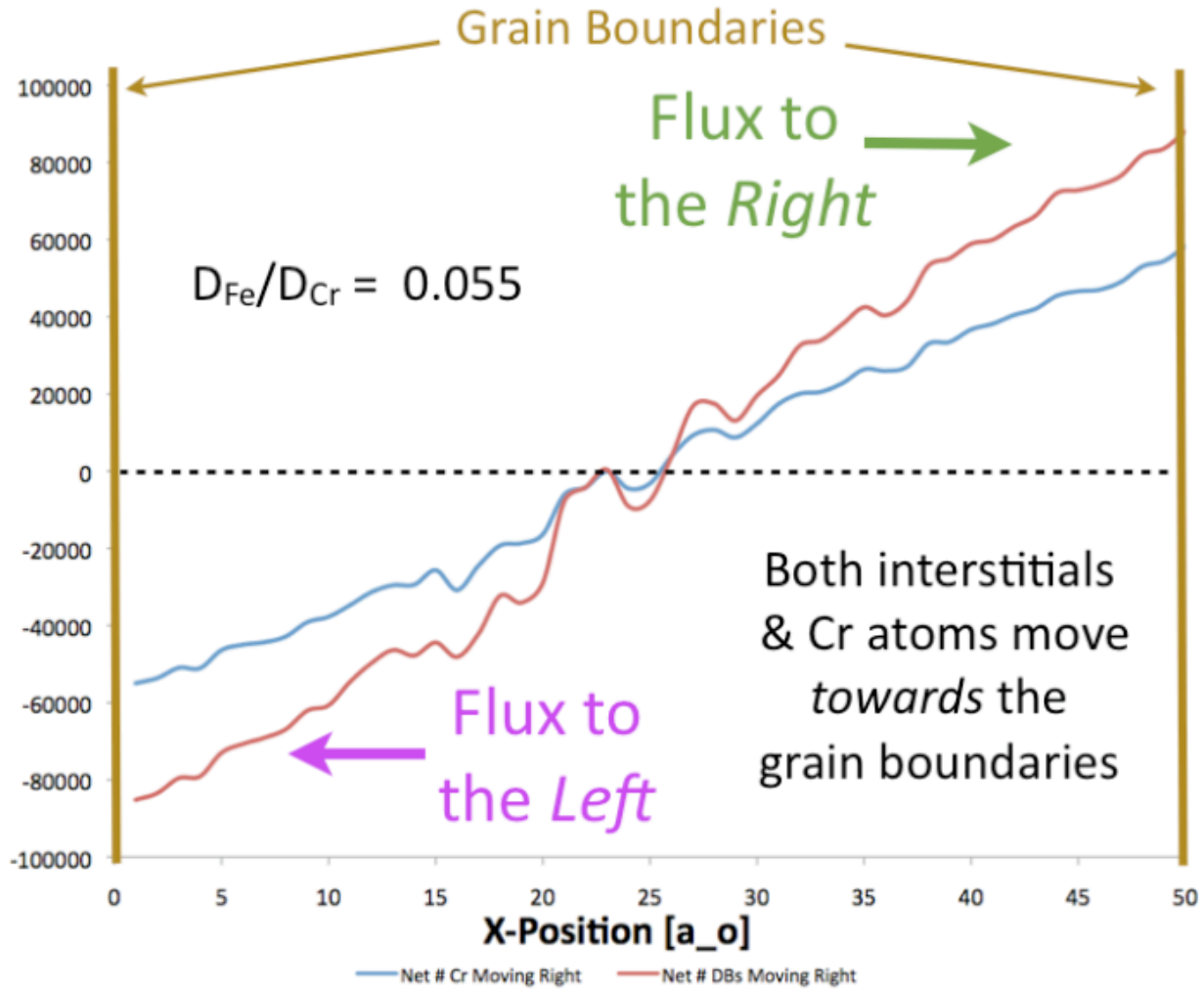

Figure 3.5. KLMC model predictions of the net flux of interstitial dumbbells (red) and Cr atoms (blue) through the simulation volume at 1000°C for electron irradiation at a dose rate of 1.3×10^{-5} dpa/sec and a dose of 4 dpa. The results show a strong coupling of the interstitial and Cr atom flux. An Fe to Cr diffusivity ratio of 0.055 was obtained, for which about 65% of the atomic flux moving in the same direction as the interstitials was Cr versus about 35% for Fe.

4.0 Summary and Conclusions

This project developed a systematic experimental and modeling approach to determining Cr RIS in F-M alloys. It was experimentally determined that the austenitic alloy D9 exhibited Cr depletion, as was expected for an austenitic steel. The magnitude of RIS reached a steady-state value of ~3 wt% by 10 dpa.

The F-M alloys exhibited much different behavior. T91 exhibited Cr enrichment that increased up to 7 dpa, and then decreased between 7 dpa and 10 dpa. This behavior was observed at both 400°C and 500°C. HT9 and HCM12A also exhibited complex RIS behavior with Cr enrichment at 400°C and 3 dpa, then changing to Cr depletion at 7 dpa and 10 dpa. The complex dose dependence of the F-M alloys is attributed to microstructural evolution during irradiation. The magnitude of RIS in F-M alloys decreased with temperature above 400°C. At all proton irradiation doses studied, the magnitude Cr RIS in T91, between 400°C and 500°C, either decreased, or remained within the error of one another. The Fe^{++} ion irradiations yielded a similar result for T91, with the magnitude of Cr enrichment decreasing between 440°C and 600°C.

The temperature and bulk Cr concentration dependence of the experimental results was shown to be in agreement with those dependencies predicted by the Inverse Kirkendall model. However, the IK model is unable to predict the more complex dose dependence observed in experiments.

Two distinctly different kinetic lattice Monte Carlo (KLMC) models were developed within this project to simulate the coupling between point defect and solute fluxes to a planar sink. This enabled identification and quantification of the corresponding radiation-induced segregation of Cr in BCC Fe-Cr alloys by vacancy- or interstitial-mediated transport mechanism, respectively. Each of these models used lattice-based semi-empirical Finnis-Sinclair N-body potentials to calculate the lattice potential energy associated with individual solute exchanges with point defects, with the specific potential chosen to best agree with ab-initio data which showed that Cr binds with both interstitial dumbbells and vacancies, albeit the interaction with the vacancy is quite weak. The KLMC simulations reveal that:

- Cr has a higher diffusivity than Fe by a vacancy mechanism and the corresponding atomic flux of Cr is larger than Fe in the opposite direction to the vacancy flux;
- Cr concentration at grain boundaries decreases as a result of vacancy transport during electron or proton irradiation, consistent with the Inverse Kirkendall model;
- Inclusion of other point defect sinks into the KLMC simulation of vacancy-mediated diffusion only influences the results in the low temperature, recombination dominated regime, but does not change the conclusion that Cr depletes as a result of vacancy transport to the sink;
- Cr segregation behavior is independent of Frenkel pair versus cascade production, as simulated for electron versus proton irradiation conditions, for the temperatures investigated;
- The amount of Cr depletion at the planar boundary with vacancy-mediated diffusion reaches an apparent saturation value by about 1 dpa, with the precise saturation concentration dependent on the ratio of Cr to Fe diffusivity; and

- Cr diffuses faster than Fe by an interstitial transport mechanism, and the corresponding atomic flux of Cr is much larger than Fe in the same direction as the interstitial flux.

These results confirm the possibility that the mixed enrichment and depletion behavior of radiation-induced Cr segregation might be explained based on the differences in interstitial versus vacancy fluxes to a given boundary. However, additional modeling work is required to fully quantify the anticipated Cr segregation behavior as a function of grain boundary character and irradiation conditions.

5.0 Publications and Presentations

5.1 Publications

J.P. Wharry, Z. Jiao, and G.S. Was. *Application of the Inverse Kirkendall Model of Radiation-Induced Segregation to Ferritic-Martensitic Alloys*. Journal of Nuclear Materials, under review.

Z. Jiao and G.S. Was. *Precipitate Evolution in Ion Irradiated HCM12A*. Journal of Nuclear Materials, under review.

J.P. Wharry, Z. Jiao, V. Shankar, G.S. Was, and J.T. Busby. *Radiation-Induced Segregation and Phase Stability in Ferritic-Martensitic Alloys*. Journal of Nuclear Materials, in press.

Z. Jiao, V. Shankar, and G.S. Was. *Phase Stability in Proton and Heavy Ion Irradiated Ferritic-Martensitic Alloys*. Journal of Nuclear Materials, accepted.

G.S. Was, J.P. Wharry, B. Frisbie, B.D. Wirth, D. Morgan, J.D. Tucker, and T.R. Allen. *Assessment of Radiation-Induced Segregation Mechanisms in Austenitic and Ferritic-Martensitic Alloys*. Journal of Nuclear Materials, 411 (2011) 41.

Z. Jiao and G.S. Was. *Segregation Behavior in Proton- and Heavy Ion-Irradiated Ferritic-Martensitic Alloys*. Acta Materialia, 59 (2011) 4467.

Z. Jiao, V. Shankar, J. Wharry, and G. Was. *Phase Stability in Proton and Heavy Ion Irradiated Ferritic-martensitic Alloys*. Transactions of the American Nuclear Society, 102 (2010) 824.

S. Choudhury, L. Barnard, D. Morgan, K. Field, T. Allen, J.P. Wharry, Z. Jiao, G. Was, and B. Wirth. *Radiation Induced Segregation in Ferritic-martensitic Steels*. Transactions of the American Nuclear Society, 102 (2010) 715.

K.L. Wong, H.-J. Lee, J.-H. Shim, B. Sadigh, and B.D. Wirth, "Multiscale modeling of point defect interactions in Fe-Cr alloys", *J. Nucl. Mater* **386-388** (2009) 227-230.

Z. Jiao, J. Penisten, G. Was, and R. Martens. *Atom Probe Tomography of Radiation-Induced Precipitation in Ferritic-Martensitic Alloy HCM12A*. Microscopy and Microanalysis, Volume 15, Supplement S2 (2009) 1374.

5.2 Conference presentations

J.P. Wharry, Z. Jiao, and G.S. Was. *Application of Inverse Kirkendall Model of Radiation-Induced Segregation to Ferritic-Martensitic Alloys*. The Minerals, Metals & Materials Society Annual Meeting, San Diego, CA, 2011.

B. Frisbie, B.D. Wirth, G.S. Was, and J.P. Wharry, *Lattice Kinetic Monte Carlo Simulations of Radiation Induced Segregation of Chromium in Ferritic-Martensitic Steels*. The Minerals, Metals & Materials Society Annual Meeting, San Diego, CA, 2011.

Z. Jiao, J.P. Wharry, G.S. Was, C. Ling, and A. Van der Ven. *Ni-Si Phases in Irradiated Austenitic Steels*. Materials Research Society Fall Meeting, Boston, MA, 2010.

B. Frisbie and B.D. Wirth *Kinetic Lattice Monte Carlo Simulations of Radiation Induced Segregation of Chromium in Ferritic-Martensitic Steels*. Materials Research Society Fall Meeting, Boston, MA, 2010.

Z. Jiao, J. Michalicka, J.P. Wharry, and G.S. Was. *Irradiated Microstructure of Austenitic and Ferritic-Martensitic Steels at High Fluences*. Materials Science & Technology, Houston, TX, 2010.

G.S. Was, J.P. Wharry and B. Wirth. *Radiation-induced Segregation in Austenitic and Ferritic-martensitic Steels*. 12th International Conference on Modern Materials and Technologies (CIMTEC), 5th Forum on New Materials, Montecatini Terme, Italy, 2010.

Z. Jiao, V. Shankar, J.P. Wharry, and G.S. Was. *Phase Stability in Proton and Heavy Ion Irradiated Ferritic-Martensitic Alloys*. Nuclear Fuels and Structural Materials for Next Generation Nuclear Reactors, Embedded Topical in American Nuclear Society Annual Meeting, San Diego, CA, 2010.

Z. Jiao, V. Shankar, J.P. Wharry, and G.S. Was. *Irradiation Microstructure and Hardening in Ferritic-Martensitic Alloys*. Nuclear Fuels and Structural Materials for Next Generation Nuclear Reactors, Embedded Topical in American Nuclear Society Annual Meeting, San Diego, CA, 2010.

S. Choudhury, L. Bernard, D. Morgan, K. Field, T. Allen, J. Wharry, Z. Jiao, G. Was and B. Wirth. *Radiation-Induced Segregation in Ferritic/Martensitic Steels*. Nuclear Fuels and Structural Materials for Next Generation Nuclear Reactors, Embedded Topical in American Nuclear Society Annual Meeting, San Diego, CA, 2010.

Z. Jiao, J.P. Wharry, V. Shankar, G.S. Was and J.T. Busby. *Radiation-Induced Segregation and Phase Stability in Ferritic-Martensitic Alloys*. International Conference on Fusion Reactor Materials, Sapporo, Japan, 2009.

S. Dwaraknath and B.D. Wirth. *Atomistic Simulation of a<100> Dislocation Loop Formation Mechanisms in Irradiated Ferritic Alloys*. . International Conference on Fusion Reactor Materials, Sapporo, Japan, 2009.

Z. Jiao, J.P. Wharry, G.S. Was and R.L. Martens. *Atom Probe Tomography of Radiation-Induced Precipitation in Ferritic-Martensitic Alloy HCM12A*. Microscopy & Microanalysis Meeting, Richmond, VA, 2009.

J.S. Penisten, Z. Jiao and G.S. Was. *Radiation-Induced Segregation in Ferritic-Martensitic Alloys HT9, T91, and HCM12A*. The Minerals, Metals & Materials Society Annual Meeting, San Francisco, CA, 2009.

Milestone Status: Year 3

Milestone/Task Description	Percent Complete	Completion Date
Microstructure meas. on series #2 irradiation,	100%	Q11
Irradiation series #3 (Fe^{++} at high dose)	100%	Q12
Hardness measurement	100%	Q11
Microstructure measurement on series #3 irradiations	100%	Q12
Development of atomic-scale kinetic Monte Carlo model to simulate Cr RIS	100%	Q11
Kinetic Monte Carlo modeling of Cr RIS + comparison with MIK rate theory model of Cr/Si RIS as a function of temperature and dose	100%	Q12
Kinetic Monte Carlo + rate theory modeling of interstitial dislocation loop evolution as a function of temperature and dose	100%	Q12
Comparison to in-reactor data	100%	Q12
Final report	100%	Q13

Budget Data

			Approved Spending Plan	Actual Spent
Phase / Budget Period			Total	Total
	From	To		
Year 1	October 2007	September 2008	200,000	161,150
Year 2	October 2008	September 2009	200,000	206,329
Year 3	October 2009	March 2011	200,000	232,521
		Totals	600,000	599,945